

# Substrate-Induced Changes in the Dynamics of Rhodopsin Kinase (G Protein-Coupled Receptor Kinase 1)

Tivadar Orban,<sup>†</sup> Chih-chin Huang,<sup>‡</sup> Kristoff T. Homan,<sup>‡</sup> Beata Jastrzebska,<sup>†</sup> John J. G. Tesmer,<sup>\*,‡,§</sup> and Krzysztof Palczewski<sup>\*,†</sup>

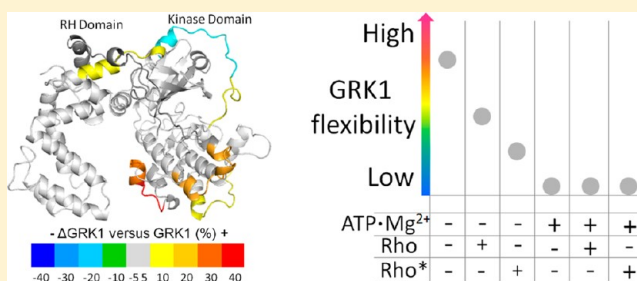
<sup>†</sup>Department of Pharmacology, School of Medicine, Case Western Reserve University, Cleveland, Ohio 44106-4965, United States

<sup>‡</sup>Life Sciences Institute, 210 Washtenaw Avenue, University of Michigan, Ann Arbor, Michigan 48109-2216, United States

<sup>§</sup>Department of Pharmacology, 210 Washtenaw Avenue, University of Michigan, Ann Arbor, Michigan 48109-2216, United States

## S Supporting Information

**ABSTRACT:** G protein-coupled receptor (GPCR) kinases (GRKs) instigate the desensitization of activated GPCRs via phosphorylation that promotes interaction with arrestins, thereby preventing the interaction of GPCRs with heterotrimeric G proteins. A current proposed model of GRK1 activation involves the binding of activated rhodopsin (Rho\*) to the N-terminal region of GRK1. Perhaps concomitantly, this N-terminal region also stabilizes a closed, active conformation of the kinase domain. To further probe this model, we mapped changes in the backbone flexibility of GRK1 as it binds to its two substrates, adenosine triphosphate (Mg<sup>2+</sup>·ATP) and Rho\*. We found that the conformational flexibility of GRK1 was reduced in the presence of either Mg<sup>2+</sup>·ATP or Rho\*, with Mg<sup>2+</sup>·ATP having the greatest effect. In a truncated form of GRK1 lacking the N-terminal region (ΔN-GRK1), peptides that directly interact with ATP were not as dramatically stabilized by adding Mg<sup>2+</sup>·ATP, and dynamics were greater in the interface between the large lobe of the kinase domain and the regulator of the G protein signaling homology domain. In the presence of Mg<sup>2+</sup>·ATP, the influence of Rho\* versus Rho on GRK1 dynamics was negligible.



Normal visual function relies on the ability of rhodopsin (Rho) to respond to light stimuli and then quickly return to the dark-adapted state.<sup>1</sup> Recovery of the dark state is in part orchestrated by G protein-coupled Rho receptor (GPCR) kinase 1 (GRK1), which desensitizes activated rhodopsin (Rho\*)<sup>2,3</sup> by docking to and phosphorylating residues in the C-terminal tail of the receptor.<sup>4–7</sup> This phosphorylation in turn promotes an interaction with the capping protein, arrestin, that blocks subsequent interactions with transducin.<sup>4</sup> Humans lacking GRK1 suffer from so-called Oguchi disease,<sup>8</sup> experiencing normal light adaptation at low levels of ambient light but abnormally slow dark adaptation at high levels of illumination.<sup>9</sup> We hypothesized that without a functional GRK1 in vivo, decay of Rho\* to opsin and regeneration with 11-*cis*-retinal probably would constitute the sole pathway for recovering rod sensitivity.<sup>9</sup> In mice, inactivation of the GRK1 gene eliminates light-dependent phosphorylation of Rho\*, resulting in a larger and longer-lasting single-photon response than in wild-type animals.<sup>10</sup>

The currently proposed mechanism of GRK1 activation is believed to consist of two distinct steps. Rho\* first binds to the ~19 N-terminal residues of the kinase, inducing the formation of an  $\alpha$ -helix (Figure 1). This helix then interacts with the kinase domain in a manner that bridges the large and small lobes and stabilizes a more closed, active conformational state. The importance of the 19 N-terminal amino acid residues for

activation of GRK1 has already been described.<sup>11,12</sup> Truncation of this N-terminal region in GRK1, GRK2, or GRK5 abolished receptor phosphorylation.<sup>12–14</sup> Moreover, mutation of residues in the small lobe of the GRK kinase domain that interact directly with the N-terminal helix, as observed in the structure of GRK6 in a relatively closed conformation,<sup>15</sup> greatly compromised GPCR phosphorylation.<sup>16</sup>

To probe this model for GRK activation further, we used deuterium exchange mass spectrometry (DXMS) to characterize the structural flexibility of GRK1 in the presence or absence of its substrates. We hypothesized that in the presence of Mg<sup>2+</sup>·ATP we should observe changes in the overall flexibility consistent with multiple crystal structures of GRK1 in complex with ATP and/or ADP. Moreover in the presence of Rho\*, we should observe changes in the stability of the 19 N-terminal amino acids of GRK1 and perhaps in regions of the protein kinase with which this region interacts.<sup>15</sup> As a control, we used a GRK1 molecule lacking the first 19 amino acid residues (ΔN-GRK1). We found that both Mg<sup>2+</sup>·ATP and Rho\* induced marked reductions in the flexibility of GRK1, whereas deletion

Received: March 1, 2012

Revised: April 4, 2012

Published: April 5, 2012

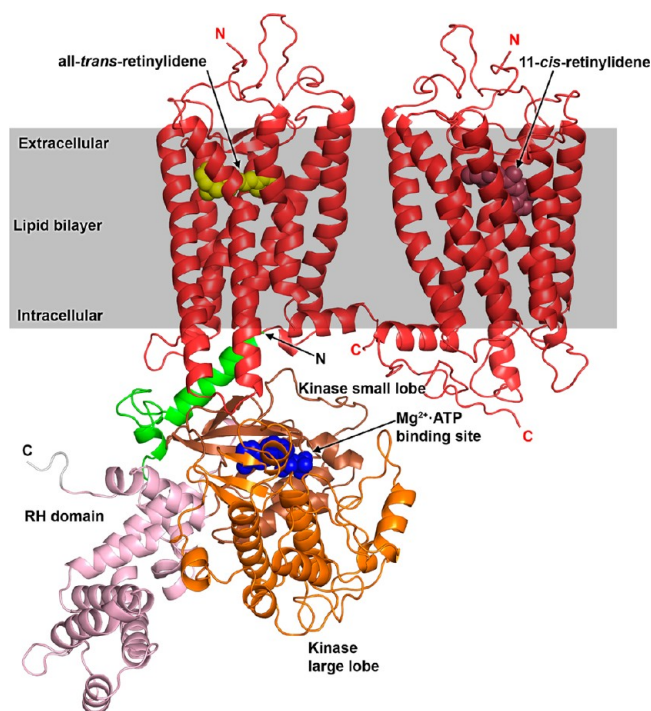


**Figure 1.** Model of the Rho–GRK1 complex. GRK1 modeled in a closed conformation with an ordered N-terminal helix is docked to Rho\* using the C-terminal helix of  $G\alpha_s$  present in the  $\beta_2AR$ – $G_s$  crystal structure as a guide.<sup>16,33</sup> The coordinates for the model, in Protein Data Bank format, are available upon request. Positions of the ordered N- and C-termini are labeled with N and C, respectively. Domains of GRK1 are colored as follows: green for the N-terminal region (Ser<sup>1</sup>–Pro<sup>42</sup>), pink for the RH domain (Pro<sup>43</sup>–Glu<sup>184</sup> and Trp<sup>515</sup>–Arg<sup>532</sup>), brown for the small lobe of the kinase domain (Asp<sup>185</sup>–Asn<sup>268</sup>), and orange for the large lobe of the kinase domain (Gly<sup>269</sup>–Pro<sup>514</sup>). The C-terminal region of GRK1 is colored gray. The GRK1 model was constructed using a homology modeling strategy based on the GRK6 X-ray structure.<sup>15</sup> The expected position of the lipid bilayer relative to the Rho\*–GRK1 complex is illustrated by the gray rectangle. In this cartoon, a theoretical Rho\*–Rho heterodimer is colored red, based on the recently modeled H8–H8 dimer orientation, although monomeric Rho is also an efficient substrate for GRK1 in vitro.<sup>34–36</sup> All-trans-retinylidene and 11-cis-retinylidene are depicted using yellow and brown spheres, respectively.

of the 19 N-terminal amino acids resulted in increased flexibility in the active site and interdomain contacts of this enzyme.

## EXPERIMENTAL PROCEDURES

**Expression and Purification of Bovine GRK1 and  $\Delta N$ -GRK1.** High-Five cells were infected with viruses encoding residues 1–535 of GRK1 (hence lacking the C-terminal farnesylation site) or  $\Delta N$ -GRK1 (residues 20–535) for 48 h prior to being harvested and purified as described previously.<sup>16,17</sup> Both proteins were engineered to have C-terminal hexahistidine tags. Briefly, cell pellets were resuspended in lysis buffer [20 mM HEPES (pH 7.5) containing 150 mM NaCl and 10 mM  $\beta$ -mercaptoethanol] supplemented with phenylmethanesulfonyl fluoride and leupeptin. Cells were homogenized and lysed via sonication, and debris was pelleted by ultracentrifugation. The soluble fraction was loaded onto a Ni-NTA column, washed with lysis buffer supplemented with 10 mM imidazole, and eluted with lysis buffer containing 200 mM imidazole at pH 7.5. Protein-containing fractions were pooled, diluted to reduce the NaCl concentration to <50 mM, and

loaded onto a Source15S ion exchange column (GE Healthcare, Piscataway, NJ). The column was eluted with an increasing NaCl gradient (0 to 500 mM), and the protein eluted between 100 and 200 mM NaCl. Fractions containing the protein were pooled, concentrated, and loaded onto a tandem S200 size exclusion column (GE Healthcare) pre-equilibrated with 20 mM HEPES (pH 7.5) containing 50 mM NaCl and 2 mM DTT. All purification steps were performed at 4 °C. Purified protein was then aliquoted, flash-frozen in liquid nitrogen, and stored at –80 °C for future use.

**Preparation of Rod Outer Segment (ROS) Membranes.** ROS membranes were prepared from 100 bovine retinas under dim red light by using discontinuous sucrose gradients as described previously.<sup>18</sup> Membranes were diluted in 40 mL of hypotonic buffer [5 mM Bis-Tris propane (BTP) (pH 7.5) containing 0.1 mM EDTA and 1 mM DTT], and proteins were released by gentle homogenization followed by centrifugation at 25000g and 4 °C for 30 min. This extraction procedure was repeated three times. Combined membranes were suspended in 3 mL of 10 mM BTP (pH 7.5) and 100 mM NaCl and either used immediately or frozen at –80 °C. Rho concentrations were determined from their absorption at 500 nm by using an extinction coefficient  $\epsilon$  of 40600 M<sup>–1</sup> cm<sup>–1</sup>.<sup>18</sup>

**Amide Hydrogen–Deuterium Exchange of GRK1 and  $\Delta N$ -GRK1.** Hydrogen–deuterium exchange experiments were performed as follows. Ten micrograms of GRK1 in 10 mM HEPES (pH 7.5) containing 0.15 M NaCl and 1 mM DTT was incubated in 80  $\mu$ L of D<sub>2</sub>O on ice for 10, 20, 30, 60, 300, 600, and 1800 s. After each incubation, deuterium exchange was terminated by adding 10  $\mu$ L of quench solution (D<sub>2</sub>O with the pH adjusted to 2.4 with HCl). Immediately thereafter, 10  $\mu$ L of pepsin (1.7 mg/mL; Worthington, Lakewood, NJ) was added to the solution. The final pH was 2.5. Then the sample was digested for 8 min on ice before the resulting peptides were injected on a Luna 20 mm  $\times$  2.00 mm C18 column (Phenomenex, Torrance, CA) with a temperature-controlled autosampler set to 4 °C attached to a Hewlett-Packard 1100 HPLC system (Agilent Technologies, Santa Clara, CA). Peptides were eluted with the following gradients: from 0 to 4 min, 98% H<sub>2</sub>O in 0.1% (v/v) formic acid (A) and 2% 2-propanol in 0.1% (v/v) formic acid (B); from 4 to 12 min, from 98 to 2% A. Peptides were directed into a Finnigan LXQ instrument (Thermo Finnigan, Waltham, MA) equipped with an electrospray ionization source operating at 300 °C. MS<sup>2</sup> spectra were collected after collision-induced dissociation of ions with a normalized collision energy set to 35 eV. Deuterium exchange experiments conducted in the presence of Mg<sup>2+</sup>·ATP were performed as described for apo-GRK1. Concentrations of ATP and Mg<sup>2+</sup> were 1 and 2 mM, respectively.

**Amide Hydrogen–Deuterium Exchange of GRK1 and  $\Delta N$ -GRK1 in the Presence of Rho or Rho\*.** These experiments were initiated after either GRK1 or  $\Delta N$ -GRK1 had been mixed with either ROS or photoactivated ROS membranes [1:2 (w/w) GRK1:Rho]. ROS membranes were activated with light (150 W) delivered by fiber light through a 480–520 nm band-pass filter for 30 s. Hydrogen–deuterium exchange was performed in the dark. D<sub>2</sub>O was exposed in a manner similar to that described for GRK1 in the absence of Rho. Before digestion with pepsin, samples were terminated with quenching solution (pH 2.4) supplemented with 1 mM Mg<sup>2+</sup> and 1 mM Ca<sup>2+</sup> chloride salts. All digestions were conducted in tubes wrapped with aluminum foil. Then they were centrifuged at 10000g for 30 s. This additional step, as

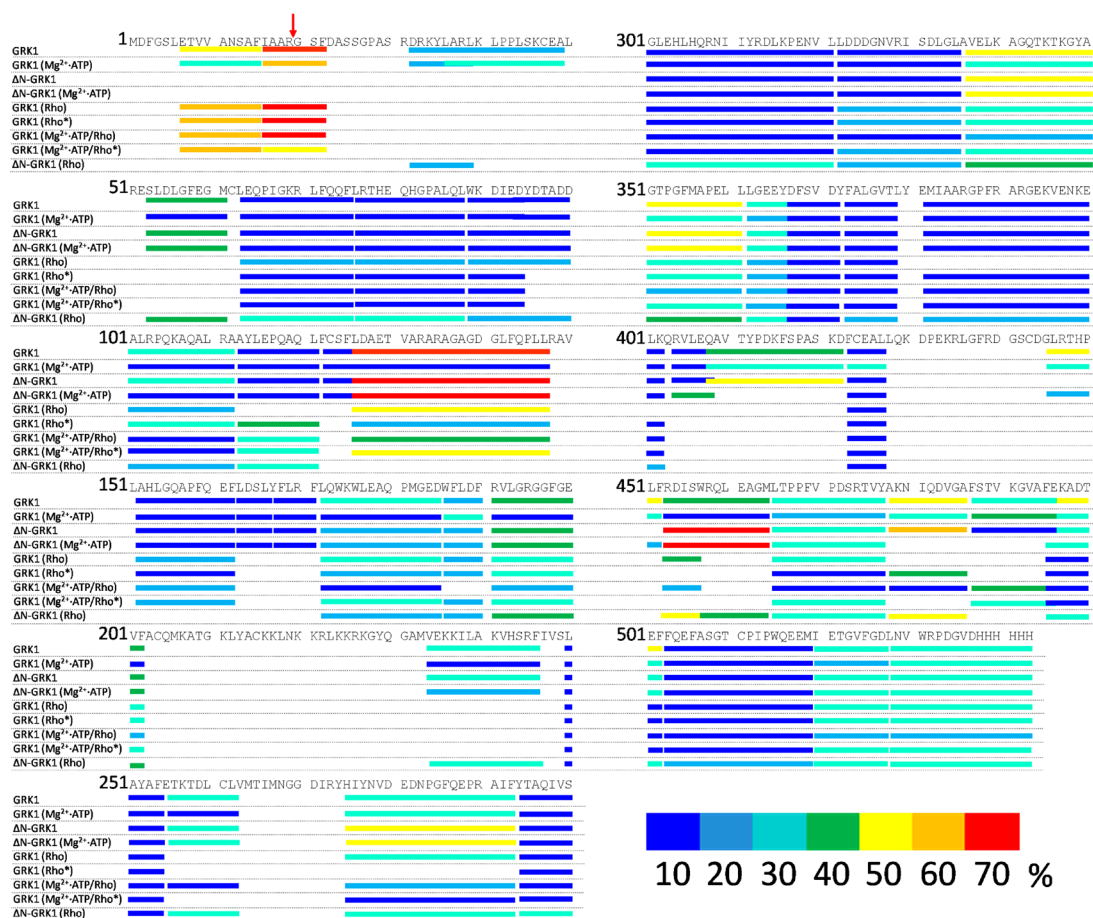


**Figure 2.** Proteolytic cleavage of GRK1 or ΔN-GRK1 by pepsin with deuterium uptake mapped on the primary sequence. Peptide coverage after proteolytic digestion of bovine GRK1 by pepsin is mapped on the primary sequence of the kinase. Peptide fragments identified by MS<sup>2</sup> following an 8 min digestion resulted in 96% coverage. Normalized deuterium uptake was evaluated according to the flowchart presented in Figure 3 and described in Experimental Procedures. Uptake is color-coded as follows: 0–10%, dark blue; 10–20%, blue; 20–30%, cyan; 30–40%, green; 40–50%, yellow; 50–60%, orange; 60–70%, red. The red arrow indicates the position of the N-terminus of ΔN-GRK1.

compared to the procedure described above for apo-GRK1, was included to pellet ROS membranes. Supernatants were collected and processed as described above for apo-GRK1 samples.

Before starting production-run experiments, we first evaluated the effects of adding 1 mM Mg<sup>2+</sup> and 1 mM Ca<sup>2+</sup> to the quench solution for Rho and Rho\* samples. The effect of this combination was first investigated on the uptake of deuterium by GRK1. This control was critical because we had observed that addition of Mg<sup>2+</sup> in D<sub>2</sub>O used to dilute samples caused significant conformational changes in apo-GRK1 (vide infra). In all the experiments described here, the pH was maintained at 2.5. Addition of 1 mM Mg<sup>2+</sup> and 1 mM Ca<sup>2+</sup> to the pH 2.4 quench solution had no detectable effect on the uptake of deuterium by apo-GRK1 (data not shown), allowing us to compare the deuterium uptake profile of GRK1 with profiles obtained in the presence of Rho or Rho\*.

**Mass Spectrometry of Pepsin Digests.** Peptides resulting from digestion with pepsin were identified on the basis of their MS<sup>2</sup> spectra compared to their theoretical y and b ions. First, the raw files format (Thermo Finnigan) was converted to an mzXML file format through instrument-associated software. Then the resulting files were searched against the primary sequences of GRK1 and ΔN-GRK1 (Figure 2) with the MassMatrix search engine.<sup>19</sup> The quality of each

peptide search was evaluated by estimating three statistical scores, namely, pp, pp<sub>2</sub>, and p<sub>tag</sub> described in detail elsewhere.<sup>20</sup> Each deuterated peptide was identified by using both its retention time (minutes) and the charge state of its undeuterated control counterpart.

**Analysis of Deuterium Exchange Products.** Undeuterated signals were identified by MS<sup>2</sup> as emanating from bona fide GRK1 peptic fragments by comparing the theoretical peptide product ions to ions obtained after collision-induced dissociation of the specific ion. Deuterated peptides were additionally identified by their retention times as described above. Eluted peaks were processed in a semiautomatic fashion whereby the peak envelope and the consequent centroid were evaluated with HDEExpress.<sup>21</sup> For each peptic peptide, we calculated the maximal theoretical number of exchangeable protons. For Pro-containing peptides, the maximal exchangeable number was decreased by one for each Pro residue. Protons of amino acid residue side chains have very rapid exchange rates and thus were not included. Whereas deuterium exchange at peptide bond sites is expected during the dilution procedure, peptide deuteriums located on amino acid side chains also are exchanged with protons during the liquid chromatography step. The total percent of deuterium uptake was evaluated for each peptide and represented with Origin 8 SR0 version 8.0725 (OriginLab Corp., Northampton, MA)

(Figure 3C) as a function of D<sub>2</sub>O incubation time as described in detail elsewhere.<sup>22</sup> Error bars represent standard errors of the

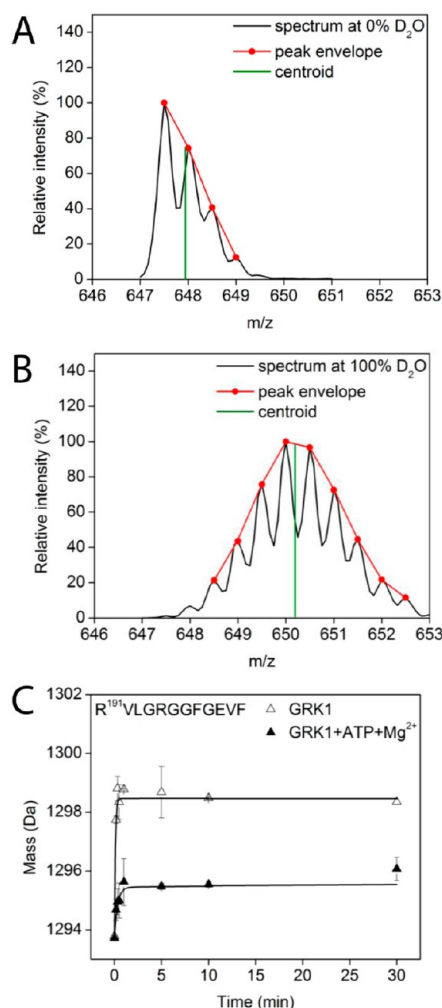


**Figure 3.** Typical workflow for evaluation of hydrogen–deuterium exchange. (A) Spectrum of a doubly charged peptide with the sequence R<sup>191</sup>VLGRGGFGEVF. For the purpose of illustration, the peak envelope is colored red whereas the centroid calculated by using the algorithm described in Experimental Procedures is colored green. (B) Same peak at the same retention time as the undeuterated species in panel A. (C) Typical deuterium uptake of the R<sup>191</sup>VLGRGGFGEVF peptide under two different experimental conditions. The absolute mass of the R<sup>191</sup>VLGRGGFGEVF peptide as a function of incubation time is shown by the open triangles for apo-GRK1 and closed triangles for Mg<sup>2+</sup>-ATP-loaded GRK1.

means (SEM), with statistical significance assessed by the Student's *t* test. Data from triplicate experiments were averaged. Deuterium exchange was color-coded on the basis of the total percent of the theoretical maximal deuterium uptake defined for each peptide: 0–10%, dark blue; 10–20%, light blue; 20–30%, cyan; 30–40%, green; 40–50%, yellow; 50–60%, orange; 60–70%, red. Color-coded molecular models illustrating deuterium exchange profiles were created with Pymol and Chimera.<sup>23</sup>

**Molecular Modeling.** Because there are no crystal structures of GRK1 in a closed state in which its 19 N-terminal amino acids are ordered, molecular models of GRK1 and ΔN-GRK1 were generated with the Modeler modeling package.<sup>24</sup> Primary sequences of GRK1 and ΔN-GRK1 (Figure 2)

together with the X-ray structure of GRK6 in complex with sangivamycin<sup>15</sup> were used as input parameters for the modeling procedure. Models were visually interpreted using Pymol.<sup>25</sup>

**Statistical Analyses.** Graphical and statistical analyses were conducted with Origin 8 SR0. Error bars represent SEM. Data were derived from at least three independent experiments.

## RESULTS

**Dynamics of Apo- and Mg<sup>2+</sup>-ATP-Loaded GRK1.** After incubation in D<sub>2</sub>O, regions buried in the hydrophobic core of apo-GRK1 had limited deuterium uptake (Figure 4, blue), i.e.,

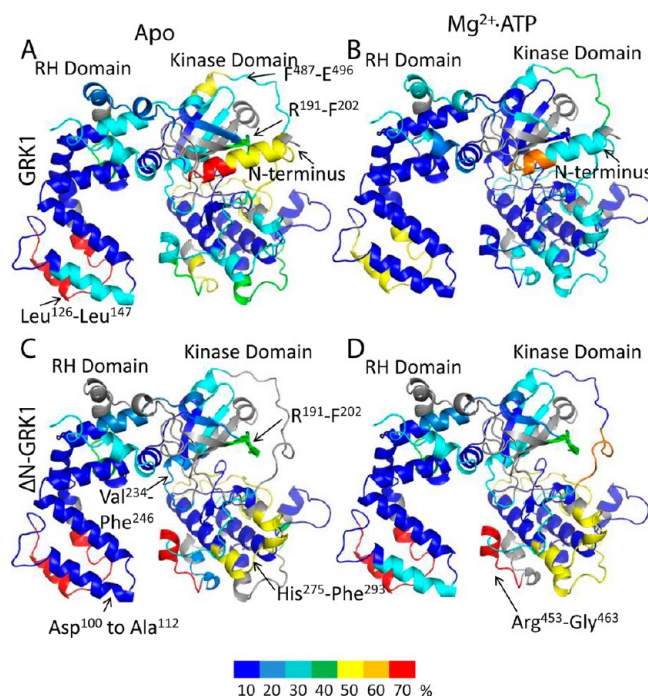


**Figure 4.** Normalized hydrogen–deuterium uptake by GRK1 and ΔN-GRK1. Color coding based on the normalized deuterium uptake was mapped onto the three-dimensional model of GRK1 as described in Molecular Modeling. Color coding is as described in the legend of Figure 2. For ΔN-GRK1, the N-terminal helix was removed from the model. Normalized deuterium uptake for (A) apo-GRK1, (B) GRK1 in the presence of Mg<sup>2+</sup>-ATP, (C) apo-ΔN-GRK1, and (D) ΔN-GRK1 in the presence of Mg<sup>2+</sup>-ATP. Regions where uptake was not determined because it was below the detection threshold or peptide signals overlapped are colored gray.

<10% of the theoretical maximum (see Analysis of Deuterium Exchange Products). Regions in the vicinity of the Mg<sup>2+</sup>-ATP binding site, the active site tether (AST) loop that passes adjacent to the active site, and the regulator of G protein signaling homology (RH) domain were found to have increased levels of amide hydrogen exchange, i.e., >50% of the theoretical maximum (Figure 4A). The highly conserved Mg<sup>2+</sup>-ATP binding motif (P-loop) was fully characterized by the R<sup>191</sup>VLGRGGFGEVF peptide. As expected from previous studies, the N-terminus was found to be highly disordered (>40% uptake). Incubation of GRK1 with Mg<sup>2+</sup>-ATP significantly decreased the level of deuterium uptake in all peptide fragments, consistent with the dramatic thermostabilization observed for GRK1 upon binding ATP.<sup>26</sup> The highly dynamic regions that were observed in apo-GRK1 exhibited exchange rates of <10% in most locations in the

presence of  $\text{Mg}^{2+}$ -ATP. The one region that still had more than 50% exchange was located in the RH domain between residues Leu<sup>126</sup> and Leu<sup>147</sup> (Figure 4B), corresponding to the  $\alpha 6$  helix and  $\alpha 6$ – $\alpha 7$  loop of the RH domain. The high deuterium exchange rates of this region are consistent with its relatively high temperature factors in crystal structures of GRK1 in complex with ATP.<sup>17</sup> GRK1 autophosphorylation sites are found at residues Ser<sup>488</sup> and Thr<sup>489</sup>, which are included in the F<sup>487</sup>STVKGVAFE peptide. This peptide showed increased levels of deuterium uptake in the  $\text{Mg}^{2+}$ -ATP-bound form as compared to the apo form (Figures 2 and 4A,B). Interestingly, the level of uptake of deuterium by the 22 N-terminal amino acids was also reduced by the addition of  $\text{Mg}^{2+}$ -ATP, suggesting that this region folds against the kinase most of the time.

**Dynamics of Apo- $\Delta\text{N}$ -GRK1 and  $\text{Mg}^{2+}$ -ATP-Loaded  $\Delta\text{N}$ -GRK1.** Apo- $\Delta\text{N}$ -GRK1 exhibited a deuterium uptake pattern similar to that of apo-GRK1 for most regions with the following exceptions. Arg<sup>453</sup>–Gly<sup>463</sup>, which immediately precedes the AST loop, exhibited decreased flexibility in GRK1 after addition of  $\text{Mg}^{2+}$ -ATP but appeared to be unaffected by  $\text{Mg}^{2+}$ -ATP binding in the  $\Delta\text{N}$ -GRK1 molecule (Figure 4C,D). Arg<sup>191</sup>–Phe<sup>202</sup>, the P-loop, remained highly dynamic even after incubation of  $\text{Mg}^{2+}$ -ATP with  $\Delta\text{N}$ -GRK1. Two other peptides that were less affected in the  $\Delta\text{N}$ -GRK1 molecule after exposure to  $\text{Mg}^{2+}$ -ATP consisted of Val<sup>234</sup>–Phe<sup>246</sup> within the active site and His<sup>275</sup>–Phe<sup>293</sup>, which docks with the AST region in the closed structure of GRK6. The proximity of these peptides to the active site suggests that the N-terminal region of GRK1 contributes to stabilization of the ATP-bound state of the enzyme. However, we were unable to measure a difference in thermostability between wild-type GRK1 and  $\Delta\text{N}$ -GRK1 either with or without  $\text{Mg}^{2+}$ -ATP, nor were we able to show that ATP binds with different affinities to these enzymes (Figure S1 of the Supporting Information). Thus, the differences in deuterium exchange exhibited by wild-type GRK1 and  $\Delta\text{N}$ -GRK1 in the presence of  $\text{Mg}^{2+}$ -ATP may reflect the ability of the kinase to sample the closed state (Figure 1) rather than changes in the affinity for the nucleotide.

Remarkably, the peptide spanning the  $\alpha\text{J}$  helix, residues 452–464, exhibited a much higher level of deuterium exchange in  $\Delta\text{N}$ -GRK1 than in GRK1, regardless of the presence of  $\text{Mg}^{2+}$ -ATP, suggesting a more labile RH–kinase domain interface in  $\Delta\text{N}$ -GRK1. Indeed, in one structure of GRK1 (Protein Data Bank entry 3C50<sup>17</sup>), the N-terminus, which is deleted in  $\Delta\text{N}$ -GRK1, was observed to pack into the cavity between the RH and kinase domains. Thus, the N-terminus of GRK1 may help fix the RH–kinase domain interface when GRK1 is not engaged with a receptor or lipid membranes.

**Dynamics of GRK1 in the Presence of Rho and Rho\*.** Addition of Rho to apo-GRK1 did not appear to induce dramatic changes in deuterium uptake, consistent with the fact that Rho is not in an activated state. Notably, no differences were observed for the 22 N-terminal amino acids (cf. Figures 4A and 5A). Addition of Rho\* to apo-GRK1 led to a generally decreased overall level of deuterium uptake compared to that of Rho, but not at the N-terminus (Figure 5A,B). This result would be consistent with a requirement for adenine nucleotides or their analogues to be located in the active site pocket before the receptor docking competent state of GRK1 can be achieved. Interestingly, the N-terminal region (Asp<sup>7</sup>–Phe<sup>22</sup>) exhibited a higher level of deuterium exchange in the presence of Rho or Rho\* compared to apo-GRK1 (cf. Figures 4A and 5A,B). The effects observed in this experiment could be caused

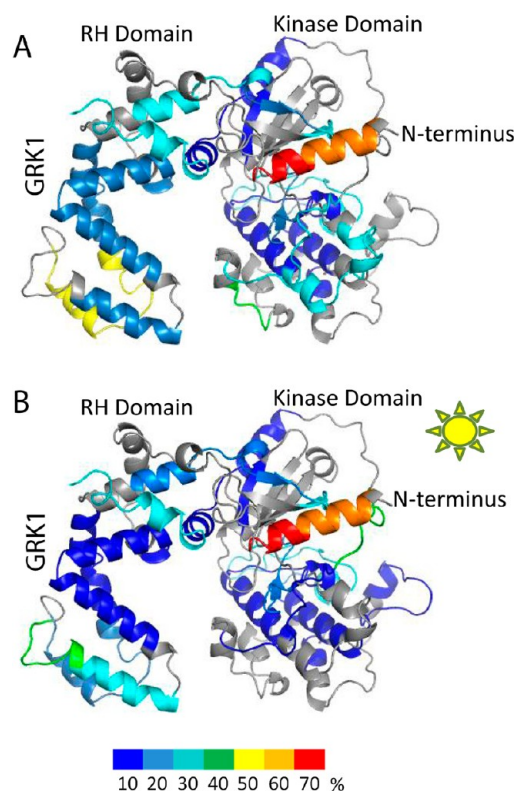


**Figure 5.** Normalized hydrogen–deuterium uptake by GRK1 in the presence of Rho and Rho\*. (A) Normalized deuterium uptake mapped onto the model of GRK1 in the presence of Rho. (B) Normalized deuterium uptake in the presence of Rho\*. Color coding is as described in the legend of Figure 2.

by interactions of GRK1 with membranes, Rho, or Rho\*. Thus, one interpretation is that the N-terminal region of GRK1 interacts nonspecifically and transiently with Rho and/or lipids, as opposed to an intramolecular interaction, prior to activation by Rho\*.

**Dynamics of  $\text{Mg}^{2+}$ -ATP-Loaded GRK1 in the Presence of Rho and Rho\*.** Here we observed reduced levels of uptake of deuterium by GRK1 in the presence of either Rho or Rho\* (Figure 6A,B). The differences between these states were negligible for most peptides studied. An exception was the region between Leu<sup>126</sup> and Leu<sup>147</sup>, which is poorly ordered in most GRK1 crystal structures and exhibited many changes from experiment to experiment reported here. Thus, it is difficult to assess whether the changes in this poorly conserved region are physiologically relevant. The presence of Rho\* in  $\text{Mg}^{2+}$ -ATP-loaded GRK1 seemed to inhibit deuterium uptake in the N-terminal Ile<sup>16</sup>–Phe<sup>22</sup> peptide (Figure 6A,B). The difference in uptake was  $\sim 30\%$  compared to that of  $\text{Mg}^{2+}$ -ATP-loaded GRK1 in the presence of Rho. In contrast, the uptake of the Asp<sup>7</sup>–Phe<sup>15</sup> peptide remained unaffected by light activation (Figure 6A,B).

**Dynamics of  $\Delta\text{N}$ -GRK1 in the Presence of Rho\*.** As with apo-GRK1, addition of Rho\* in ROS reduced the flexibility of  $\Delta\text{N}$ -GRK1 (Figure 7) but did not produce the same pattern of selective effects observed in GRK1. This could be attributed in part to the inability of the  $\Delta\text{N}$ -GRK1 molecule to interact efficiently with Rho\*. In the case of  $\Delta\text{N}$ -GRK1, the missing N-terminus affected deuterium uptake, not only in regions located far from the N-terminus but also in the P-loop

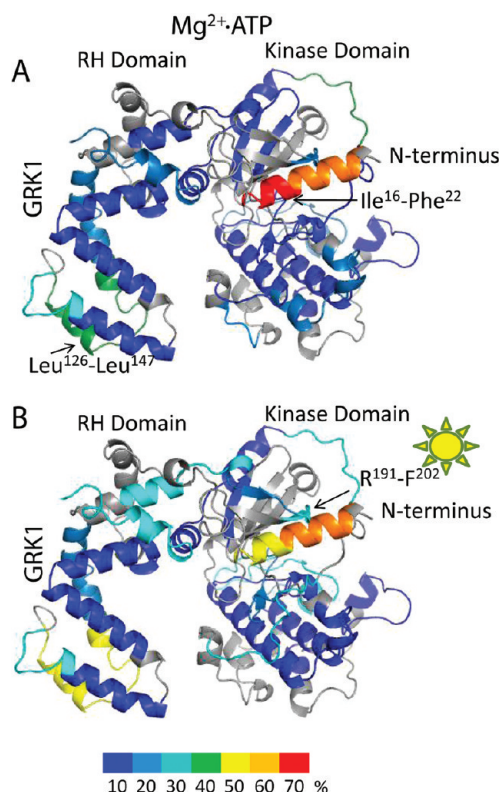


**Figure 6.** Normalized hydrogen–deuterium uptake of  $Mg^{2+}$ -ATP-loaded GRK1 in the presence of Rho and  $Rho^*$ . (A) Normalized deuterium uptake mapped on the model of GRK1 in the presence of  $Mg^{2+}$ -ATP and Rho. (B) Normalized deuterium uptake in the presence of  $Mg^{2+}$ -ATP and  $Rho^*$ . Color coding is as described in the legend of Figure 2.

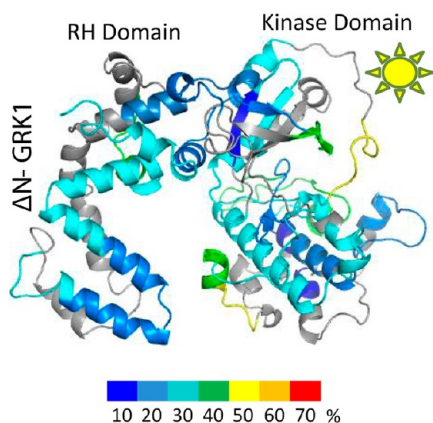


**Figure 7.** Normalized hydrogen–deuterium uptake by  $\Delta N$ -GRK1 in the presence of  $Rho^*$ . Color coding is as described in the legend of Figure 2.

(residues Arg<sup>191</sup>–Phe<sup>202</sup>), as observed for  $\Delta N$ -GRK1 in other liganded states (Figures 4C,D and 8A).

## DISCUSSION

In this study, we found that residues 1–535 of GRK1 contain regions of considerable flexibility, as do many globular proteins, and that this flexibility was reduced in the presence of either of its substrates: the nucleotide complex  $Mg^{2+}$ -ATP or the protein  $Rho^*$ . Stability was further enhanced when both substrates were added. A truncated form of GRK1 missing the first 19

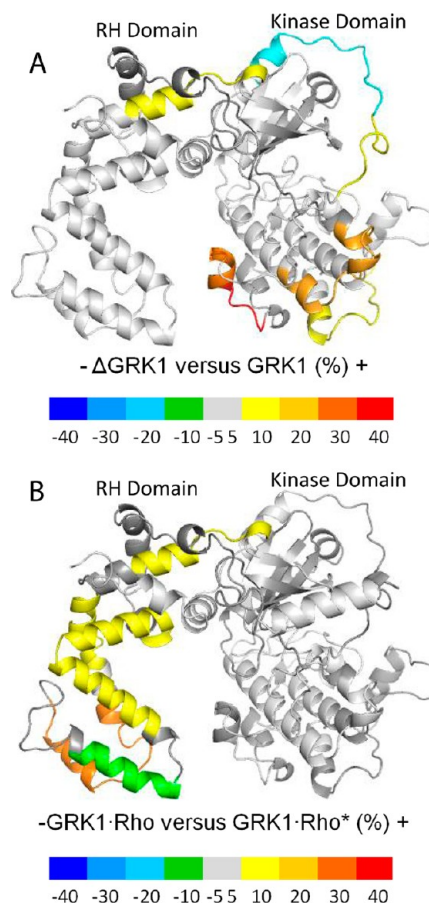


**Figure 8.** Differences in normalized hydrogen–deuterium exchange. (A) Differences in normalized deuterium uptake between  $\Delta N$ -GRK1 and apo-GRK1. (B) Differences in normalized deuterium uptake by GRK1 in the presence of either Rho or  $Rho^*$ . Color coding was assigned on the basis of the value of the difference between the normalized deuterium uptake values between the states shown. Negative differences (associated with blue, cyan, light blue, and green) denote higher levels of uptake in the case of GRK1 (A) or when  $Rho^*$  is present (B). Positive differences (associated with yellow, orange, and red) denote higher levels of uptake in  $\Delta N$ -GRK1 (A) or when Rho is present (B). Regions that have absolute differences of <10% or were not included in the analysis are colored gray.

amino acid residues,  $\Delta N$ -GRK1, failed to display most of these effects, implying that the first 19 amino acids help to dictate the overall dynamics of GRK1 in the presence of either  $Mg^{2+}$ -ATP or  $Rho^*$ .

**Effects of Rho or  $Rho^*$  on GRK1 Dynamics.** We noted that uptake of deuterium by GRK1 (Figure 4A) differed from the pattern observed when dark-adapted Rho purified from membranes was added to the mix (Figure 5A). However, GRK1 should selectively recognize only  $Rho^*$ . Thus, the observed differences could reflect a residual interaction of GRK1 with Rho or with the membrane. Upon exposure to light, however, we expected that GRK1 would interact with  $Rho^*$ , which in turn would either cause reduced flexibility of the GRK1 secondary structure or directly hinder deuterium uptake in segments involved in their interface. Indeed, we did find a decrease in the level of deuterium uptake in GRK1 following addition of  $Rho^*$  when compared to Rho (Figure 8B). One N-terminal peptide (Ile<sup>16</sup>–Phe<sup>22</sup>) showed a decreased level of uptake ( $\sim 30\%$ ) when GRK1 was incubated in the presence of  $Mg^{2+}$ -ATP and  $Rho^*$  when compared to that of

GRK1 in the presence of Rho or Rho\* alone. However, the other N-terminal peptide (Asp<sup>7</sup>–Phe<sup>15</sup>) failed to show large differences expected to result from binding site protection. These results could be due to the high flexibility of this region or to the fact that GRK1 is thought to rapidly dissociate from Rho\*, such that the differences in deuterium exchange are too small to be detected under the conditions used for our experiments. Indeed, the interaction of GRK1 with Rho\* is not as stable as that of transducin,<sup>27</sup> and isolation of a stable GRK1–Rho\* complex has not yet been reported. Moreover, GRK1 does not form so-called “extra-Meta II” in which the Meta II state of Rho\* is stabilized at the expense of other photoactivation products.<sup>27,28</sup> In contrast, a stable complex between Rho\* and transducin has been isolated biochemically and visualized by electron microscopy using single-particle reconstruction.<sup>29,30</sup> Therefore, consistent with our hydrogen–deuterium exchange measurements, there seems to be only a small fraction of GRK1 bound to Rho\* at any given time.

When the dynamics of GRK1 and Rho or Rho\* were evaluated in the presence of Mg<sup>2+</sup>·ATP, the differences between those states were found to be negligible. Once Mg<sup>2+</sup>·ATP was bound, all other parameters that could affect deuterium uptake, such as the presence of lipid bilayers in ROS and/or Rho\*, had a minimal influence. However, there were a few regions where deuterium uptake did not follow this simple trend. For example, the Leu<sup>126</sup>–Leu<sup>147</sup> region is one of the most flexible regions in the GRK1 molecule, and even when Mg<sup>2+</sup>·ATP was bound, this region exchanged up to 40–50% of the theoretical maximum (Figure 4). This held true for all our preparations of GRK1 (>50% uptake), except when Rho\* was present and Mg<sup>2+</sup>·ATP was absent (~20%) (Figure 5B). The decrease in the level of deuterium uptake following addition of Mg<sup>2+</sup>·ATP in peptides that encompass the active site, such as the P-loop, supports the view that ATP is binding as predicted by prior crystal structures. Furthermore, we could identify allosterically coupled regions that exhibit decreased levels of uptake upon binding Mg<sup>2+</sup>·ATP such as that encompassed by Asp<sup>100</sup>–Ala<sup>112</sup> (Figures 4 and 6).

When the 19 N-terminal amino acids of GRK1 were removed to create ΔN-GRK1, the most dramatic effect in the hydrogen–deuterium uptake profile compared to that of GRK1 was localized to a single region between Arg<sup>453</sup> and Met<sup>464</sup> (Figure 4C,D). This region is located at the interface between the kinase large lobe and the RH domain. It is possible that the increased level of deuterium uptake is induced by the rigid body movement of the kinase large lobe away from the RH domain, which is somehow favored in the absence of the N-terminal region. The presence of Rho\* did reduce the flexibility of ΔN-GRK1 (Figure 7) to the extent seen in the case of GRK1 when bound to Rho\*, suggesting that the N-terminal region of GRK1 is not the only region that interacts with light-activated ROS. Although the binding of ATP seems to stabilize backbone atoms in the N-terminal region of GRK1 (Figure 4A,B), this change was not associated with any measurable difference in the thermostability or affinity of ΔN-GRK1 for ATP (Figure S1 of the Supporting Information). Indeed, multiple crystal structures have been determined for GRK1 in the presence of ATP or ADP; however, the N-terminal region has not been routinely observed, nor has the kinase assumed what is considered to be a more active conformation.<sup>11,17</sup>

Before this study, GRK1 activation was proposed to involve three distinctive steps: docking of its N-terminal helix to the receptor, interaction of this helix with the kinase domain, and

kinase domain closure. These events are likely highly coupled. Our deuterium exchange results suggest that, as expected, the GRK1 molecule becomes more rigid following binding of substrates such as Mg<sup>2+</sup>·ATP and Rho\*. This agrees with the increased order and lower temperature factors in liganded states of GRK1 determined in prior crystallographic studies of GRK1.<sup>17</sup> ΔN-GRK1 did not show the same deuterium exchange pattern as intact GRK1 for all its substrates, probably because ΔN-GRK1 is unable to carry out all of the required steps believed to result in sampling the closed, more active and presumably less dynamic conformation of this kinase. Thus, our results confirm that the N-terminal region in GRKs plays a multifaceted role that could involve modulation of the interdomain contacts of GRK1 as well as its membrane lipid interactions<sup>31</sup> and receptor binding.<sup>12,32</sup>

## ■ ASSOCIATED CONTENT

### ● Supporting Information

Comparison of the thermostability and ATP affinity of GRK1 and ΔN-GRK1 (Figure S1). This material is available free of charge via the Internet at <http://pubs.acs.org>.

## ■ AUTHOR INFORMATION

### Corresponding Author

\*J.J.G.T.: Life Sciences Institute, 210 Washtenaw Ave., University of Michigan, Ann Arbor, MI 48109-2216; phone, (734) 615-9544; fax, (734) 763-6492; e-mail, [tesmerjj@umich.edu](mailto:tesmerjj@umich.edu). K.P.: Department of Pharmacology, School of Medicine, Case Western Reserve University, 10900 Euclid Ave., Cleveland, OH 44106-4965; phone, (216) 368-4631; fax, (216) 368-1300; e-mail, [kxp65@case.edu](mailto:kxp65@case.edu).

### Funding

This research was supported in part by Grants EY008061 and HL071818 from the National Institutes of Health. K.P. is the John H. Hord Professor of Pharmacology.

### Notes

The authors declare no competing financial interest.

## ■ ACKNOWLEDGMENTS

We thank Dr. Marcin Golczak for help with the MS. We also thank Dr. L. T. Webster, Jr., and members of the Palczewski laboratory for critical comments on the manuscript.

## ■ ABBREVIATIONS

AST, active site tether; BTP, Bis-Tris propane; DTT, dithiothreitol; DXMS, deuterium exchange mass spectrometry; GRK1, G protein-coupled rhodopsin kinase 1; ΔN-GRK1, GRK1 lacking the first 19 amino acids; HEPES, 4-(2-hydroxyethyl)-1-piperazineethanesulfonic acid; MS, mass spectrometry; MS<sup>2</sup>, tandem MS/MS; RH, regulator of G protein signaling homology; Rho, rhodopsin; Rho\*, photoactivated Rho; ROS, rod outer segment.

## ■ REFERENCES

- (1) Palczewski, K. (2006) G protein-coupled receptor rhodopsin. *Annu. Rev. Biochem.* 75, 743–767.
- (2) Maeda, T., Imanishi, Y., and Palczewski, K. (2003) Rhodopsin phosphorylation: 30 years later. *Prog. Retinal Eye Res.* 22, 417–434.
- (3) Arshavsky, V. Y., Lamb, T. D., and Pugh, E. N., Jr. (2002) G proteins and phototransduction. *Annu. Rev. Physiol.* 64, 153–187.
- (4) Wilden, U., Hall, S. W., and Kuhn, H. (1986) Phosphodiesterase activation by photoexcited rhodopsin is quenched when rhodopsin is

phosphorylated and binds the intrinsic 48-kDa protein of rod outer segments. *Proc. Natl. Acad. Sci. U.S.A.* 83, 1174–1178.

(5) Palczewski, K., Buczylo, J., Kaplan, M. W., Polans, A. S., and Crabb, J. W. (1991) Mechanism of rhodopsin kinase activation. *J. Biol. Chem.* 266, 12949–12955.

(6) Ohguro, H., Rudnicka-Nawrot, M., Buczylo, J., Zhao, X., Taylor, J. A., Walsh, K. A., and Palczewski, K. (1996) Structural and enzymatic aspects of rhodopsin phosphorylation. *J. Biol. Chem.* 271, 5215–5224.

(7) Ohguro, H., Van Hooser, J. P., Milam, A. H., and Palczewski, K. (1995) Rhodopsin phosphorylation and dephosphorylation *in vivo*. *J. Biol. Chem.* 270, 14259–14262.

(8) Yamamoto, S., Sippel, K. C., Berson, E. L., and Dryja, T. P. (1997) Defects in the rhodopsin kinase gene in the Oguchi form of stationary night blindness. *Nat. Genet.* 15, 175–178.

(9) Cideciyan, A. V., Zhao, X., Nielsen, L., Khani, S. C., Jacobson, S. G., and Palczewski, K. (1998) Null mutation in the rhodopsin kinase gene slows recovery kinetics of rod and cone phototransduction in man. *Proc. Natl. Acad. Sci. U.S.A.* 95, 328–333.

(10) Chen, C. K., Burns, M. E., Spencer, M., Niemi, G. A., Chen, J., Hurley, J. B., Baylor, D. A., and Simon, M. I. (1999) Abnormal photoresponses and light-induced apoptosis in rods lacking rhodopsin kinase. *Proc. Natl. Acad. Sci. U.S.A.* 96, 3718–3722.

(11) Huang, C. C., Orban, T., Jastrzebska, B., Palczewski, K., and Tesmer, J. J. (2011) Activation of G protein-coupled receptor kinase 1 involves interactions between its N-terminal region and its kinase domain. *Biochemistry* 50, 1940–1949.

(12) Palczewski, K., Buczylo, J., Lebiada, L., Crabb, J. W., and Polans, A. S. (1993) Identification of the N-terminal region in rhodopsin kinase involved in its interaction with rhodopsin. *J. Biol. Chem.* 268, 6004–6013.

(13) Yu, Q. M., Cheng, Z. J., Gan, X. Q., Bao, G. B., Li, L., and Pei, G. (1999) The amino terminus with a conserved glutamic acid of G protein-coupled receptor kinases is indispensable for their ability to phosphorylate photoactivated rhodopsin. *J. Neurochem.* 73, 1222–1227.

(14) Noble, B., Kallal, L. A., Pausch, M. H., and Benovic, J. L. (2003) Development of a yeast bioassay to characterize G protein-coupled receptor kinases. Identification of an NH<sub>2</sub>-terminal region essential for receptor phosphorylation. *J. Biol. Chem.* 278, 47466–47476.

(15) Boguth, C. A., Singh, P., Huang, C. C., and Tesmer, J. J. (2010) Molecular basis for activation of G protein-coupled receptor kinases. *EMBO J.* 29, 3249–3259.

(16) Huang, C. C., Yoshino-Koh, K., and Tesmer, J. J. (2009) A surface of the kinase domain critical for the allosteric activation of G protein-coupled receptor kinases. *J. Biol. Chem.* 284, 17206–17215.

(17) Singh, P., Wang, B., Maeda, T., Palczewski, K., and Tesmer, J. J. (2008) Structures of rhodopsin kinase in different ligand states reveal key elements involved in G protein-coupled receptor kinase activation. *J. Biol. Chem.* 283, 14053–14062.

(18) Matthews, R. G., Hubbard, R., Brown, P. K., and Wald, G. (1963) Tautomeric Forms of Metarhodopsin. *J. Gen. Physiol.* 47, 215–240.

(19) Xu, H., and Freitas, M. A. (2009) MassMatrix: A database search program for rapid characterization of proteins and peptides from tandem mass spectrometry data. *Proteomics* 9, 1548–1555.

(20) Xu, H., and Freitas, M. A. (2007) A mass accuracy sensitive probability based scoring algorithm for database searching of tandem mass spectrometry data. *BMC Bioinf.* 8, 133.

(21) Weis, D. D., Kass, I. J., and Engen, J. R. (2006) Semi-automated analysis of hydrogen exchange mass spectra using HX-Express. *J. Am. Soc. Mass Spectrom.* 17, 1700–1703.

(22) Orban, T., Bereta, G., Miyagi, M., Wang, B., Chance, M. R., Sousa, M. C., and Palczewski, K. (2010) Conformational changes in guanylate cyclase-activating protein 1 induced by Ca<sup>2+</sup> and N-terminal fatty acid acylation. *Structure* 18, 116–126.

(23) Pettersen, E. F., Goddard, T. D., Huang, C. C., Couch, G. S., Greenblatt, D. M., Meng, E. C., and Ferrin, T. E. (2004) UCSF Chimera: A visualization system for exploratory research and analysis. *J. Comput. Chem.* 25, 1605–1612.

(24) Marti-Renom, M. A., Stuart, A., Fiser, A., Sánchez, R., Melo, F., and Sali, A. (2000) Comparative protein structure modeling of genes and genomes. *Annu. Rev. Biophys. Biomol. Struct.* 29, 291–325.

(25) DeLano, W. L. (2002) *The PyMOL Molecular Graphics System*, DeLano Scientific, San Carlos, CA.

(26) Thal, D. M., Yeow, R. Y., Schoenau, C., Huber, J., and Tesmer, J. J. (2011) Molecular mechanism of selectivity among G protein-coupled receptor kinase 2 inhibitors. *Mol. Pharmacol.* 80, 294–303.

(27) Pulvermuller, A., Palczewski, K., and Hofmann, K. P. (1993) Interaction between photoactivated rhodopsin and its kinase: Stability and kinetics of complex formation. *Biochemistry* 32, 14082–14088.

(28) Hofmann, K. P., Pulvermuller, A., Buczylo, J., Van Hooser, P., and Palczewski, K. (1992) The role of arrestin and retinoids in the regeneration pathway of rhodopsin. *J. Biol. Chem.* 267, 15701–15706.

(29) Jastrzebska, B., Tsybovsky, Y., and Palczewski, K. (2010) Complexes between photoactivated rhodopsin and transducin: Progress and questions. *Biochem. J.* 428, 1–10.

(30) Jastrzebska, B., Ringler, P., Lodowski, D. T., Moiseenkova-Bell, V., Golczak, M., Muller, S. A., Palczewski, K., and Engel, A. (2011) Rhodopsin–transducin heteropentamer: Three-dimensional structure and biochemical characterization. *J. Struct. Biol.* 176, 387–394.

(31) Pao, C. S., Barker, B. L., and Benovic, J. L. (2009) Role of the amino terminus of G protein-coupled receptor kinase 2 in receptor phosphorylation. *Biochemistry* 48, 7325–7333.

(32) Boguth, C. A., Singh, P., Huang, C. C., and Tesmer, J. J. (2010) Molecular basis for activation of G protein-coupled receptor kinases. *EMBO J.* 29, 3249–3259.

(33) Huang, C. C., and Tesmer, J. J. (2011) Recognition in the face of diversity: Interactions of heterotrimeric G proteins and G protein-coupled receptor (GPCR) kinases with activated GPCRs. *J. Biol. Chem.* 286, 7715–7721.

(34) Knepp, A. M., Periolo, X., Marrink, S. J., Sakmar, T. P., and Huber, T. (2012) Rhodopsin forms a dimer with cytoplasmic helix 8 contacts in native membranes. *Biochemistry* 51, 1819–1821.

(35) Gurevich, V. V., and Gurevich, E. V. (2008) GPCR monomers and oligomers: It takes all kinds. *Trends Neurosci.* 31, 74–81.

(36) Bayburt, T. H., Leitz, A. J., Xie, G., Oprian, D. D., and Sligar, S. G. (2007) Transducin activation by nanoscale lipid bilayers containing one and two rhodopsins. *J. Biol. Chem.* 282, 14875–14881.